Energy Engineering

Tech Science Press

DOI: 10.32604/ee.2023.028453

ARTICLE

Fault Diagnosis of Industrial Motors with Extremely Similar Thermal Images Based on Deep Learning-Related Classification Approaches

Hong Zhang[1,*], Qi Wang[1], Lixing Chen[1], Jiaming Zhou[1] and Haijian Shao[2]

[1]School of Electrical Information Engineering, Jiangsu University of Technology, Changzhou, 213001, China

[2]Department of Electrical and Computer Engineering, University of Nevada, Las Vegas, NV 89154, USA

[*]Corresponding Author: Hong Zhang. Email: hazh0216@jsut.edu.cn

Received: 19 December 2022 Accepted: 13 February 2023 Published: 07 June 2023

ABSTRACT

Induction motors (IMs) typically fail due to the rate of stator short-circuits. Because of the similarity of the thermal images produced by various instances of short-circuit and the minor interclass distinctions between categories, non-destructive fault detection is universally perceived as a difficult issue. This paper adopts the deep learning model combined with feature fusion methods based on the image's low-level features with higher resolution and more position and details and high-level features with more semantic information to develop a high-accuracy classification-detection approach for the fault diagnosis of IMs. Based on the publicly available thermal images (IRT) dataset related to condition monitoring of electrical equipment-IMs, the proposed approach outperforms the highest training accuracy, validation accuracy, and testing accuracy, i.e., 99%, 100%, and 94%, respectively, compared with 8 benchmark approaches based on deep learning models and 3 existing approaches in the literature for 11-class IMs faults. Even the training loss, validation loss, and testing loss of the eleven deployed deep learning models meet industry standards.

KEYWORDS

Induction motors; fault diagnosis; thermal images; deep learning

Nomenclature

$\frac{\partial \varepsilon_{loss}}{\partial x_l}$	The gradient
$\hat{\mathcal{R}}(x_i, \omega_i)$	The residual function
$p_{predict}(label)$	The probability distributions

1 Introduction

Various types of short-circuit failures can significantly cause motor failure in an induction motor. Because the rotor of an industrial motor generates extremely high levels of heat during operation, the conventional fault detection method necessitates invasive detection, resulting in the inability to intervene in the repair of the fault in a timely manner. Thermal imaging cameras are capable of not only measuring the temperature of thousands of points but also of converting temperature readings into thermal images. The generated thermal image can fully reflect the overall condition of the equipment

to be inspected, and the operator can easily discover that the spot pyrometer is difficult to find fine hot spots and that the infrared penetration ability is strong, can penetrate thick smoke and dense fog, and is not limited by ambient light or illumination light. Infrared thermal imaging does not use lighting or ambient light to produce scene images; instead, it relies on the radiation of the target and the background, so the infrared thermal imaging system can work 24 h a day and will not be interfered with by visible light like other night vision equipment. Low-light cameras cannot image without ambient light. However, because the pixel distribution of structured images obtained after acquisition is very similar to that of industrial motor faults, detecting faults in multiple categories is extremely difficult. For industrial rotary machinery, the development of an intelligent fault detection system that can automatically and reliably identify micro-faults that are damaging motors remains an issue that must be solved [1–3]. Although the deep learning model can extract the image's high-discrimination features, because the image is a structured description and the infrared images of different industrial motors are very similar except for a slight change in color, their shape and texture features have hardly changed. The image's low-level features have higher resolution and more position and details, and the image's high-level features have more semantic information. It is frequently overlooked and does not fully exploit the difference in color of the image on the channel.

This paper proposes a high-accuracy fault diagnosis for Industrial Motors (IMs) based on deep learning-related approaches combined with feature fusion methods; image low-level features with higher resolution and more position and details are effectively fused with high-level features with more semantic information extracted by a Gaussian filter. The remainder of this paper is organized as follows: Section 3 presents the proposed deep learning-related approach for IM fault diagnosis, such as the processing framework for classification-detection. The experiments explored based on 11 deep learning-related approaches and the performance comparison are given in Section 4, and this paper is concluded in Section 5.

2 Related Works

The classification-detection approach of the feature extraction of thermal images, BCAoID (Binarized Common Areas of Image Differences), to fault diagnosis based on thermal images can find application for protecting rotating machinery and engines, and the recognition results of the performed analysis were greater than 97.91% in the approach proposed by Glowacz [4]. For the purpose of defect identification in a three-phase induction motor, thermal image segmentation-related approaches were performed [4–9]. These approaches were based on edge detection algorithms and machine learning-related methodologies. Glowacz et al. [8] created an acoustic-based fault diagnostic technique for detecting power tool bearing and ventilation defects. According to the studies, acoustic-based analysis is useful for analyzing electrical and other mechanical faults in machines. Chen et al. [9] studied three angle grinders (AG): a healthy AG, an AG with one blocked air inlet, and an AG with two blocked air inlets. The classifier used was SMOFS-NFC (Shortened Method of Frequencies Selection Nearest Frequency Components) based on the extracted features, and the detection accuracy ranged from 89.33% to 97.33% for the three electric impact drills. Li et al. [10] introduced a fault diagnosis approach for the fault diagnosis of rotating equipment that was based on the Convolutional Neural Network (CNN) in combination with *Softmax* methods. This strategy was created to aid in the diagnosis of rotating machinery faults. The trials have shown that a variety of flaws in the rotor and bearings can be located. Karabacak et al. [11] presented the feature selection and classification for fault diagnosis of worm gearboxes (WG) under varying loading and speed conditions for the purpose of condition monitoring. The detection accuracy of the two classifications was 99.2%. He et al. [12] used infrared thermal images to collect the characteristics of the different health states of the motor. The experiments

demonstrated that even small, labeled infrared thermal images can provide an accurate diagnosis. The non-invasive method connected to infrared thermography was utilized by Choudhary et al. [13], and the identification of bearing failure at an early stage under a variety of bearing situations was carried out. Shao et al. [14,15] performed an analysis of thermal images of a rotor-bearing system under a variety of various working circumstances using a modified CNN that included transfer learning. The findings indicate that the method described was effective for the purpose of defect identification in the rotor-bearing system. Gangsar et al. [16] presented artificially intelligent (AI) methods for the detection of induction motors (IMs) in order to guarantee the continuous and problem-free operation of IMs. These approaches were developed to identify IMs. A discussion of the research gaps and future scopes in the fault monitoring and diagnosis of IMs has also been provided. This was done as an additional addition. Nath et al. [17] utilized the artificial intelligence (AI)-based rotor fault diagnosis (RFD) method to solve the issues in the health management (PHM) of the Industry 4.0 revolution. The current research and analysis in accordance with different phases of an AI-based RFD framework were also discussed. Gundewar et al. [18] provided a comprehensive review of recent developments in the condition monitoring and fault diagnosis of IMs. They also conducted an analysis of the most common faults in induction motors using time-domain, frequency-domain, and time-frequency-domain methods, as well as the application of artificial intelligence techniques for fault detection. The development of the deep learning methodologies [19–22], such as CNN-based fault diagnosis (CNFD) approaches, was thoroughly reviewed, and the further investigation by researchers into the detection of IMs was also taken into consideration.

3 Proposed Deep Learning-Related Approach for Fault Diagnosis of Industrial Motors

The main purpose of this paper is to explore the AI approach, such as the *state-of-the-art* approaches based on deep learning, to solve the fault diagnosis of IMs. In particular, the detection of categorization in this work is exceedingly difficult due to the high feature similarity across each image category. The processing diagram of the proposed approach is shown in Fig. 1. The processing framework and the experimental evaluation are the two main parts of the classification-detection process, as provided in Fig. 1.

3.1 Classification-Detection Approach Based on Deep Learning

If the number of hidden layer nodes is large sufficiently, neural networks can theoretically approximate nonlinear functions and use a large amount of data; as the amount of data increases, so does their generalization ability. This is the primary advantage of neural networks; it distinguishes them from almost all other machine learning algorithms. Deep neural networks with more than two hidden layers are not uncommon, and the number of hidden layers can be customized using a method known as hyper parameter selection. The output features of the hidden-layers in the neural network are defined by Eq. (1),

$$h_i(\boldsymbol{x})_{R^{\alpha_i-1}\to R^{\alpha_i}} = f\left(w_i^T \boldsymbol{x} + b_i\right) \tag{1}$$

where $w_i \in R^{\alpha\times\alpha_i-1}, b \in R^{\alpha_i\in N^*_{(1,+\infty)}}, f_{R\to R} \in [0,1]_{\text{sigmoid}}$ are usually a non-linear activation function. Since, the networks are prone to many types of attacks, the classification model should distinguish multi-class. Therefore, neural network with *softmax* function-based activation function could be utilized to get more accurate results. The loss function denoted as $\boldsymbol{\varepsilon}_{loss}$ is calculated by Eq. (2) based on the chain rule of gradient propagation,

$$\frac{\partial \boldsymbol{\varepsilon}_{\text{loss}}}{\partial \boldsymbol{x}_{\mathbf{l}}} = \frac{\partial \boldsymbol{\varepsilon}_{\text{loss}}}{\partial \boldsymbol{x}_{L\geq l, L\in \mathbf{N}^*}} \frac{\partial \boldsymbol{x}_{L\geq l, L\in N^*}}{\partial \boldsymbol{x}_l} = \frac{\partial \boldsymbol{\varepsilon}_{loss}}{\partial \boldsymbol{x}_{\mathbf{L}}} \left(\mathbf{1} + \frac{\partial \boldsymbol{\varepsilon}_{loss}}{\partial \boldsymbol{x}_l} \sum\nolimits_{i=1,\ldots,L-1} \mathcal{R}\left(\boldsymbol{x}_i, \omega_i\right)\right) \tag{2}$$

$$\boldsymbol{x}_{\boldsymbol{L}\geq \boldsymbol{l},\boldsymbol{L}\in \boldsymbol{N}^{*}}=\boldsymbol{x}_{0}+\sum\nolimits_{i=1,\ldots,L-1}\mathcal{R}\left(\boldsymbol{x}_{i},\omega_{i}\right) \tag{3}$$

where $\frac{\partial \boldsymbol{\varepsilon}_{\boldsymbol{loss}}}{\partial \boldsymbol{x}_{\boldsymbol{l}}}$ is the gradient that propagates over the hidden layers of deep learning model, ω_i is the model weight of the deep learning model. $\mathcal{R}$ is the residual function, and variables vector $\boldsymbol{x}_{\boldsymbol{l}}$ defined in Eq. (3) is the input feature to the lth residual unit. $\boldsymbol{L}\geq \boldsymbol{l},\boldsymbol{L}\in \boldsymbol{N}^{*}$ is a positive integer indicating the subscript of the deeper residual unit in hidden layer. As shown in Fig. 1, the skip connections related to the pre-activation module are added in the classical Residual Network (ResNet), with the recursively calculation for the $\boldsymbol{x}_{\boldsymbol{l}+\boldsymbol{1}}$ with the identity shortcut, Eq. (2) could be defined by Eq. (4),

$$\frac{\partial \boldsymbol{\varepsilon}_{\boldsymbol{loss}}}{\partial \boldsymbol{x}_{\boldsymbol{l}}}=\frac{\partial \boldsymbol{\varepsilon}_{\boldsymbol{loss}}}{\partial \boldsymbol{x}_{\boldsymbol{L}}}\left(\prod\nolimits_{i=1,\ldots,L-1}\lambda_{i}+\frac{\partial}{\partial \boldsymbol{x}_{\boldsymbol{l}}}\sum\nolimits_{i=1,\ldots,L-1}\hat{\mathcal{R}}\left(\boldsymbol{x}_{i},\omega_{i}\right)\right) \tag{4}$$

where $\hat{\mathcal{R}}\left(\boldsymbol{x}_{i},\omega_{i}\right)$ is the residual function with scalars. The feature information flow of the hidden layers will be changed exponentially when modulating scalar $\lambda_i>1$ (or $\lambda_i>1$), which is corresponding to the exponentially large (or the small even vanish). This is particularly beneficial for the backpropagated signal that passed through the weight layers. Multi-class classification uses the negative log probability as the target class and $p_{predict}(label)$ as the probability distributions as denoted by Eq. (5),

$$d\left(t_{target},p_{predict}\left(label\right)\right)=-\log p_{predict}\left(label\right)_{target} \tag{5}$$

$$Train_{in-out,\xi}\triangleq L_{out,i,\xi}=\alpha_{i}^{-1}\sum\nolimits_{\lambda=1,\ldots,\alpha_i\in N^{*}_{(1,+\infty)}}dist\left(o_{\lambda},f_{\xi}\left(i_{\lambda}\right)\right) \tag{6}$$

where t_{target} and $p_{predict}\left(label\right)$ respectively denote the target and predicted label. The decrease of loss function denoted by Eq. (6) is utilized to investigate the well-trained model based on the ideal values. for $\xi=\left(\omega_{1},b_{1},\ldots,\omega_{\alpha_i},b_{\alpha_i\in N^{*}_{(1,+\infty)}}\right)$.

3.2 Proposed Classification-Detection Approach for Fault Diagnosis of IMs

In terms of accuracy and convergence, the deep residual network outperforms ResNet as an extremely deep network framework. When skip connections and additional activations use identity mappings, the forward and backward signals can be directly passed from a block to any other block based on the calculation propagation method behind the residual building blocks. The network model facilitates training while also improving the network's generalization ability. The most popular optimization technique, such as gradient descent, is utilized to fine-tune these parameters. The advantage of a Gaussian filter is that its Fourier transform is also a Gaussian distribution centered on zero frequency (with positive and negative frequencies on both sides). The width of the filter can then be adjusted to control the effectiveness of its low-pass nature. The new features of the IMs dataset are then defined by Eq. (7),

$$f_{input}\left(\boldsymbol{x}\right)=\left\{\left\{G\left(x,\sigma_{i=1,\ldots,n}\right)*f_{i}\left(x\right)\right\}\in\mathcal{R}_{fil,Mat},f_{i}\left(x\right)\in\mathcal{R}_{ori,Mat},\mathcal{L}_{label,i}\right\}_{i=1,\ldots,n,i\in N^{*}} \tag{7}$$

where $G\left(x,\sigma_{i=1,\ldots,n}\right),f_{i}\left(x\right)$ and $\mathcal{L}_{label,i}$ are the Gaussian function, original IMs image and the corresponding class labels set, respectively. $\mathcal{R}_{fil,Mat}$ is the float matrix after filter corresponding to the original matrix space $\mathcal{R}_{ori,Mat}$. The image's low-level features have higher resolution and more position and detail information, but because they go through less convolution, they are less semantic and noisier. High-level features have more semantic information, but the resolution is low and detail perception is poor.

The main innovation of this paper is that in order to enhance the image's color, texture, and form characteristics while precisely highlighting the location, detail, and high-level features, the filtered low-level features are fused with the original features in a process referred to as fusion; the

image low-level features with higher resolution and more position and details with high-level features with more semantic information extracted by Gaussian filter are effectively fused, deep residual network is then used to extract the image's high-discrimination features, to construct the high-accuracy classification-detection approach for non-invasive fault diagnosis of IMs.

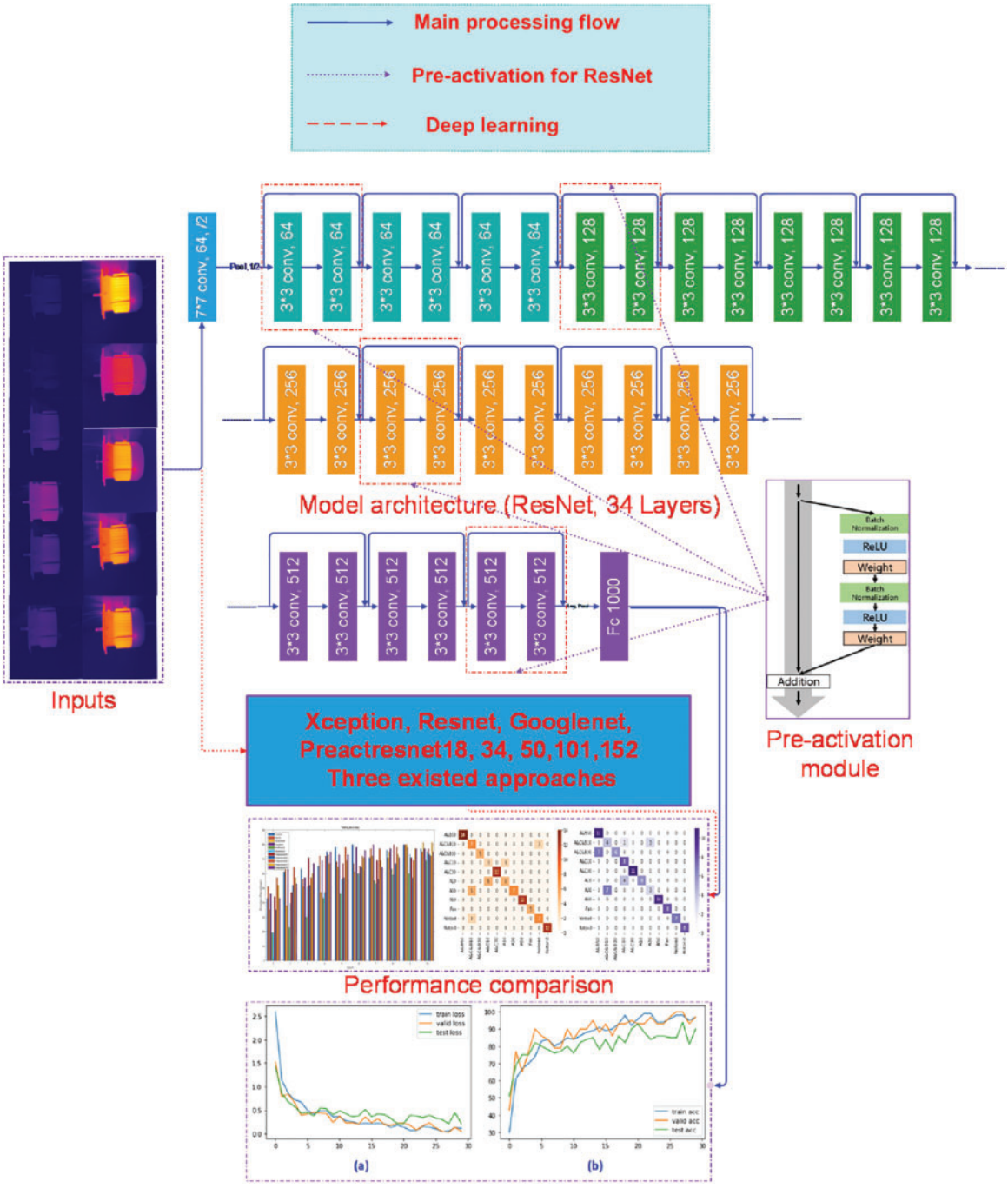

Figure 1: The processing diagram of the proposed approach

3.3 Performance Measurement Metrics of Classification-Detection Approach

In the fields of machine learning and statistical classification problems, the confusion matrix is a very useful visualization tool, particularly for the evaluation of supervised learning models. This is because the confusion matrix allows users to examine how well supervised learning models perform. The confusion matrix is a statistical metric for solving classification problems. It can be used for both binary classification and multiclass classification problems. The following Eq. (8) calculates a model's accuracy (via a confusion matrix).

$$Accuracy = \frac{TN + TP}{TN + FP + FN + TP} \tag{8}$$

where FP, FN, TP and TN represent the false positive, false negative, true positive and true negative, respectively. In other words, the matrix is a two-dimensional contingency table that can graphically display the number of false positives (FP), false negatives (FN), true positives (TP), and true negatives (TN). Instances of the actual class are represented by the matrix's columns, while certain instance predictions are represented by the matrix's rows (TN). Exceptionally useful in carrying out precise research on classification (accuracy). Since the dataset that was utilized for this study was not an imbalanced set (that is, the number of observations in the various categories varied greatly from one another), the confusion matrix was able to be used to accurately evaluate the performance of the classifier.

Additionally, because the dataset used in this paper is very comparable across the different categories, traditional machine learning techniques can yield positive results. The outcomes where the model correctly predicted the positive class, correctly predicted the negative class, incorrectly predicted the positive class, and incorrectly predicted the negative class, respectively, are denoted by the letters TP, TN, FP and FN.

4 Experiments

4.1 Thermal Images Dataset

The publicly available thermal image (IRT) dataset related to condition monitoring of electrical equipment-IMs, used for classification-detection is provided by Najafi et al. [23] (Babol Noshirvani University of Technology, Iran). This dataset contains 11 various kinds of IMs failures as well as 8 different short circuit failures, all of which are depicted by thermographic images. It is crucial to remember that all intentionally created issues are caused by internal flaws and are independent of any failures in the initial setup components or failures in any external components. In the stator windings, we take into consideration faults such as stopped rotors and cooling fan failures. The acquisition of thermal images takes place at a workbench in an Electrical Machines Laboratory using a Dali-tech T4/T8 infrared thermal imaging camera. The temperature of the surrounding environment is set at 23 degrees. The Electrical Equipment specifications is shown in Table 1.

Table 1: Electrical equipment specifications

Transformer		Induction motor	
Phase	1	Phase	Y-3
Power	1 KW	Power	1.11 KW
Voltage	220 V	Voltage	220/380 V
Input current	1.5 A	Input current	5 A

(Continued)

Table 1 (continued)

Transformer		Induction motor	
Operating voltage	220–660	Speed	2800 RPM
Frequency	50–60 Hz	Frequency	50 Hz

Thermal camera properties [23]: Dali-tech T8 TIC, Detector resolution $384 * 288$, Measurement accuracy [2%, $\gg$2%], Imaging NETD $\leqslant 0.04^{\circ}$@30°, Measuring range $[-20^{\circ}, +650^{\circ}]$, Imaging Frame Rate 50/60 Hz.

4.2 Classification-Detection Approach Based on Deep Learning

The classification problem that will be discussed in this paper belongs to a typical class of multi-class classification-detection problems. More specifically, it includes the following subproblems: A&B50 (2-phase, 50%-stator rate of short-circuit), A&C&B30 (3-phase, 30%-stator rate of short-circuit), A50, Rotor-0, Fan, A&C&30, Noload, A30, A&C&B10, A&C10 (10%, 3-phase).

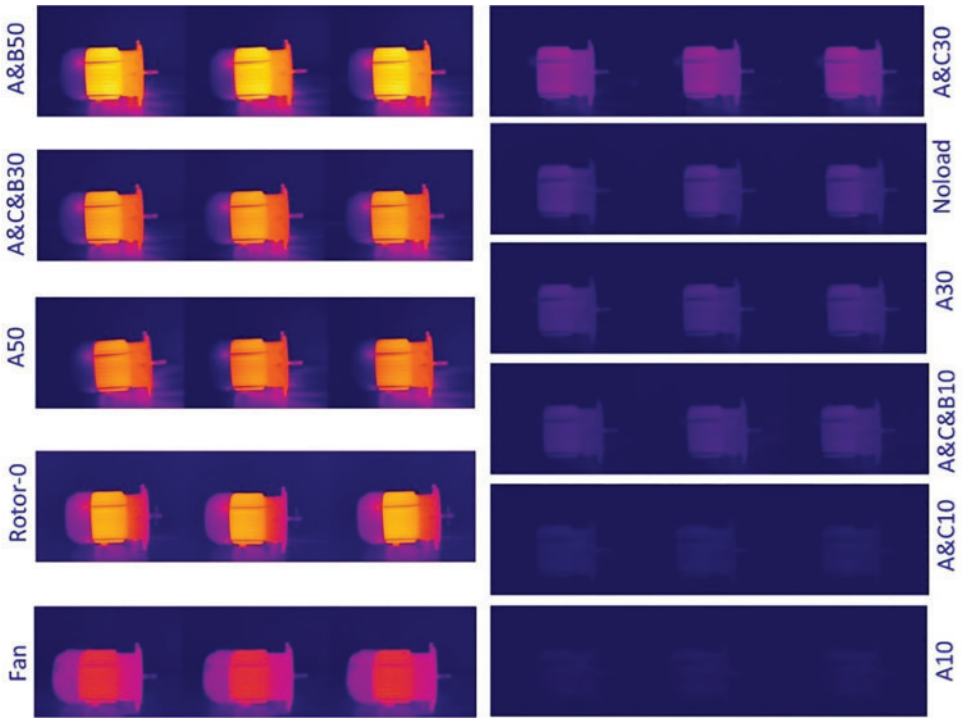

Figure 2: Samples of the IMs dataset

The sample shown in Fig. 2 depicts various industrial motor failures that fall into 11 categories. A color feature is a general feature that describes an image's or a scene's image area's surface characteristics. Usually, color features are dependent on the properties of individual pixels, with each pixel in an image or image region corresponding to a specific place within the image. The texture and shape characteristics of the 11 categories of IMs in this paper are visually compared because color is not sensitive to the direction or size of the image or image area. In particular, the classification

detection in this paper is extremely difficult because of the high similarity between IM images, i.e., the feature similarity of each category of images is extremely high. A comparison of the original and preprocessed IMs images is shown in Fig. 3. Processed images and the corresponding differences of channels (R, G, and B) are visualized in Fig. 4. If the local area and color characteristics of the image can be highlighted, the feature expression ability of the image under different channels can be effectively improved. By cascading with the original feature information, the image obtained after Gaussian filtering can effectively combine low-level features with higher resolution and more position and details with high-level features with more semantic information. It can also increase the brightness of the region of interest and improve the texture features of the motor.

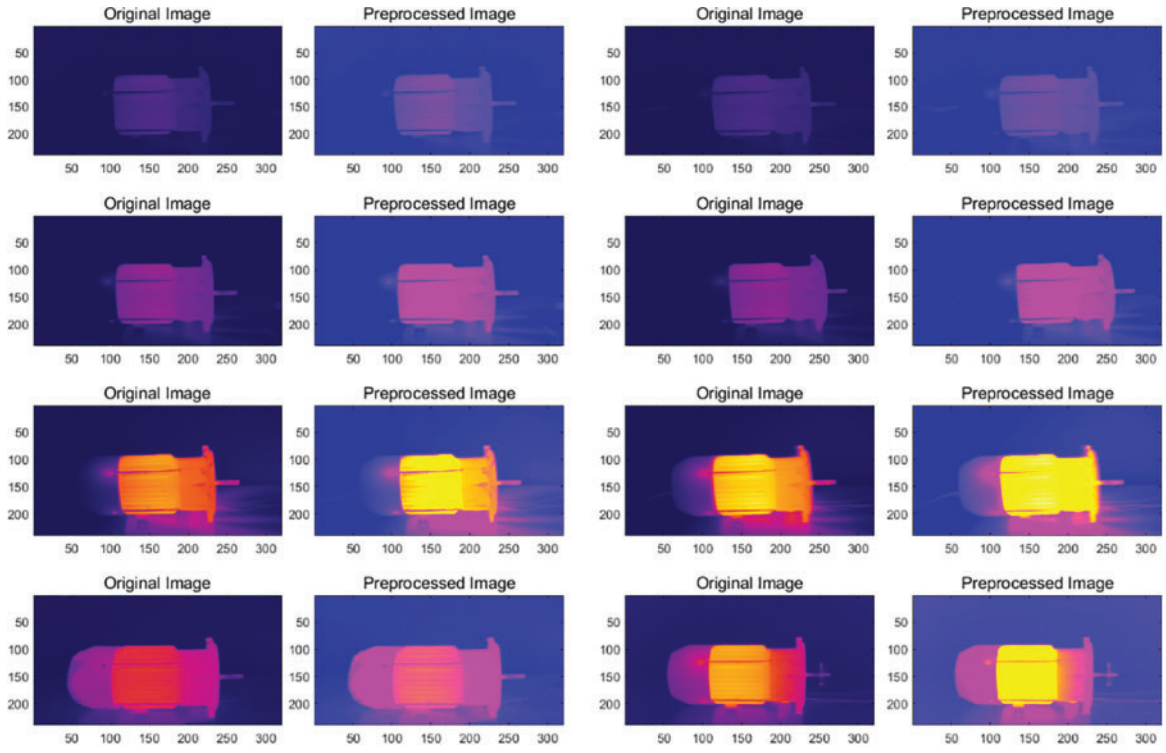

Figure 3: Comparison of original and preprocessed IMs image

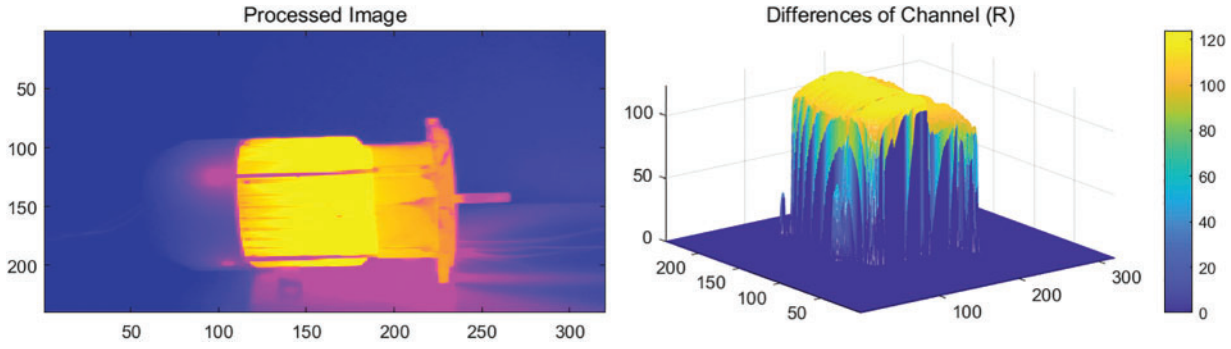

Figure 4: (Continued)

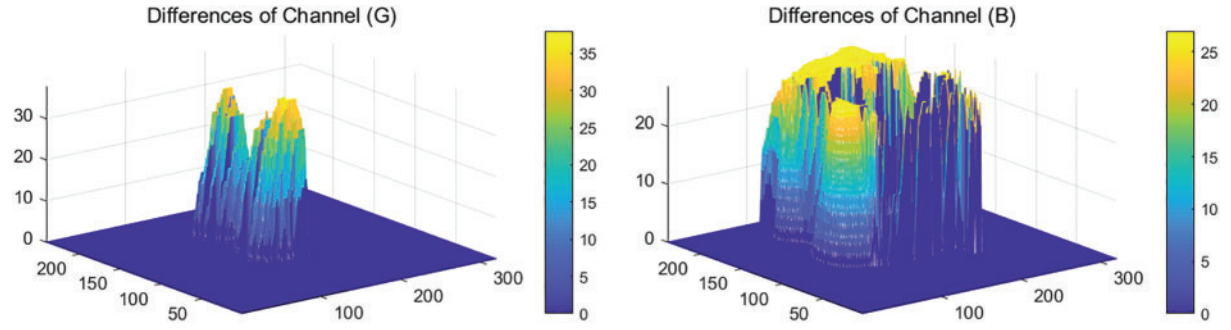

Figure 4: Processed images and the corresponding differences of channels (R, G, B)

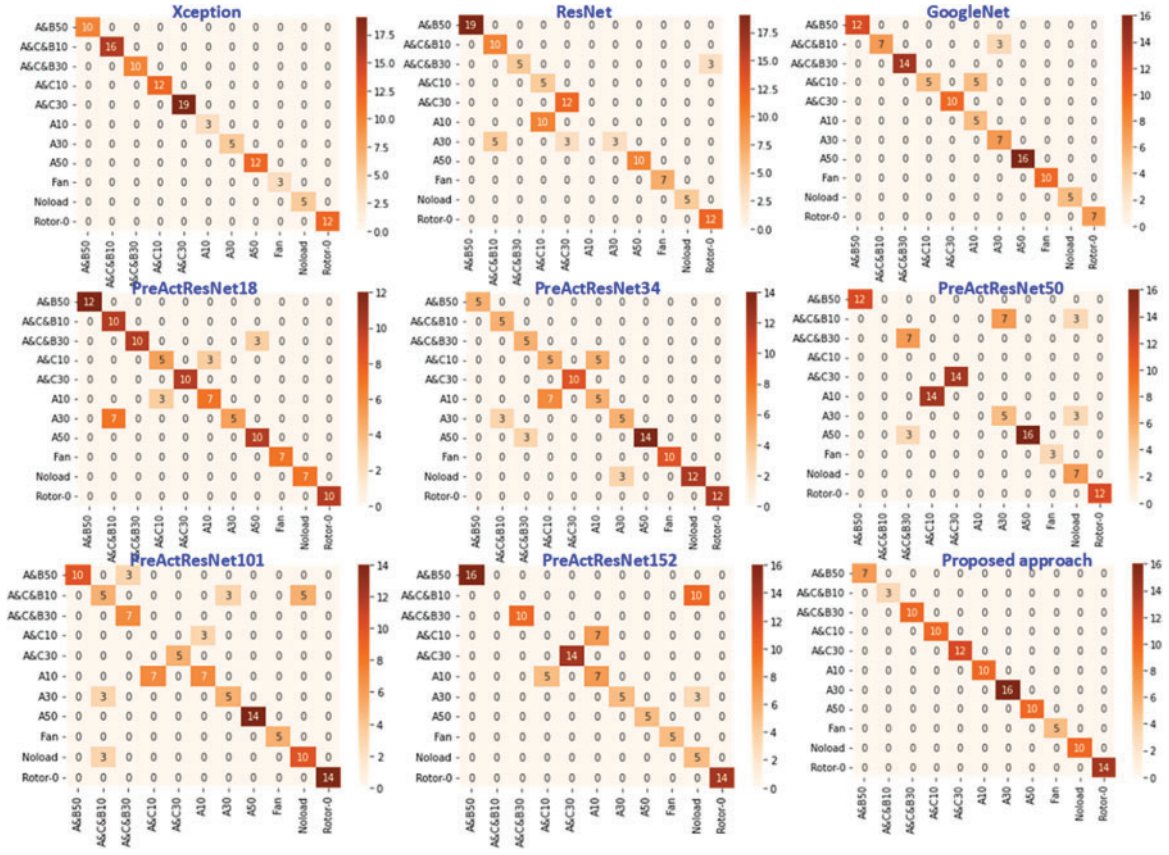

Figure 5: Confusion matrix on validation dataset

In classification detection and image accuracy evaluation, it is mainly used to compare classification results with actual measured values, and the accuracy of classification results can be displayed in a confusion matrix. The confusion matrix is calculated by comparing the position and classification of each measured cell with the corresponding location and classification in the classified image. The confusion matrix is used to observe the performance of the model in each category, and the accuracy and recall of the model corresponding to each category can be calculated. Figs. 5 and 6 show the confusion matrix for the validation and testing datasets. It is clear that the method proposed in this

paper has the lowest values of true negative and false positive, such as the correct rate of the verification set reaching 100%, while the effect on the test set is only four types (i.e., A&C&B10, A&C&B30, A10, and A30) contain a small number of fewer than three label errors, indicating that the prediction method in this paper is extremely accurate.

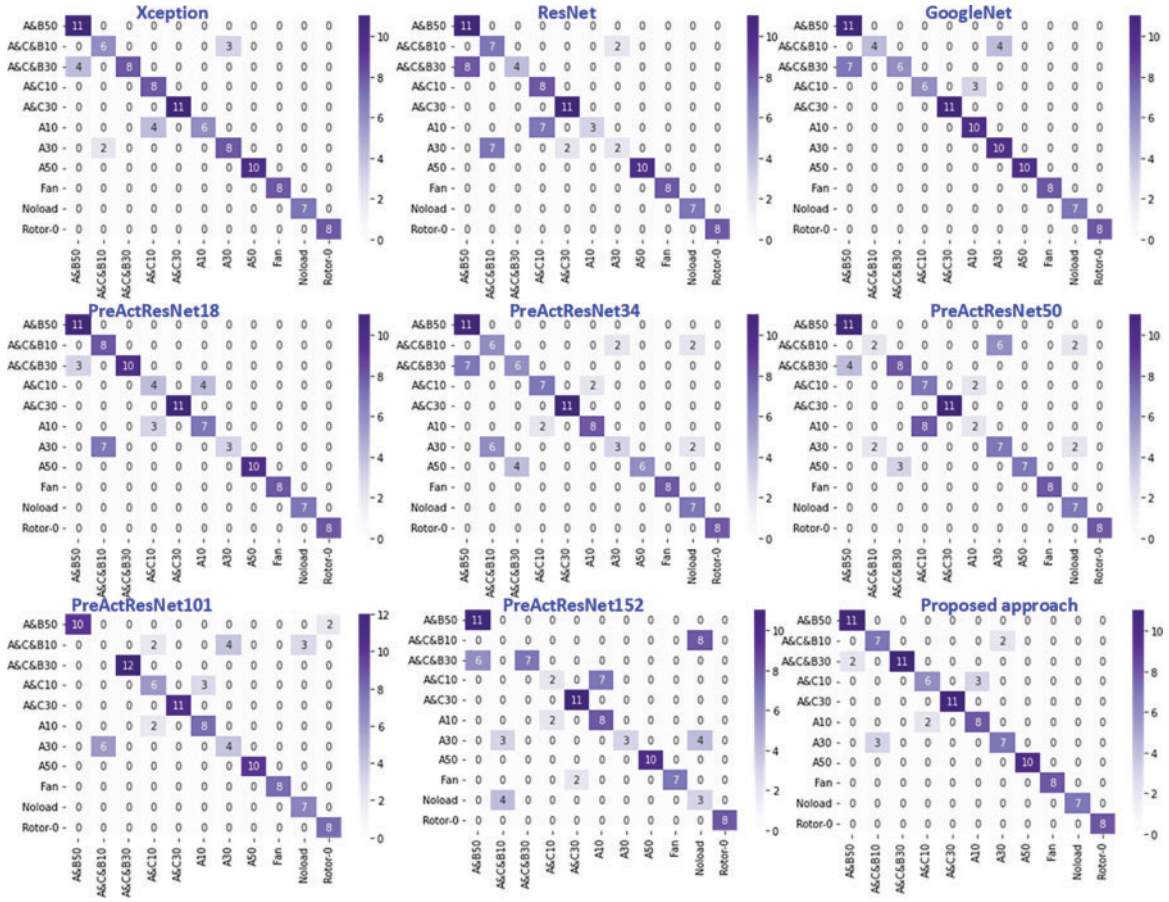

Figure 6: Confusion matrix on testing dataset

Figs. 7–9 show the statistics and boxplot (i.e., outliers and the corresponding values) of the loss of the deep learning models on training, validation, and testing datasets for a more detailed visual display. A box plot, also known as a box-and-whisker chart, box plot, or boxplot, is a statistical graphic that displays a collection of data dispersion. It is primarily used to represent the features of the original data, such as the distribution of the loss function, and may intuitively compare the distribution characteristics of other sets of loss data. This is known as classification detection and fault diagnosis. The boxplot species contains the highest, lowest, median, and two quartiles of the data. Connect the upper and lower quartiles to form the box, which should have the median in the center. Then, connect the box's upper and lower edges. The loss function measures how far the model's predicted value deviates from the true value; the better the loss function, the more effective the model is. This enables you to compare the extent of the loss caused by various categorization detection techniques visually. It is obvious from a comparison that the proposed method's loss function loss is lower and the model's classification detection performance is better.

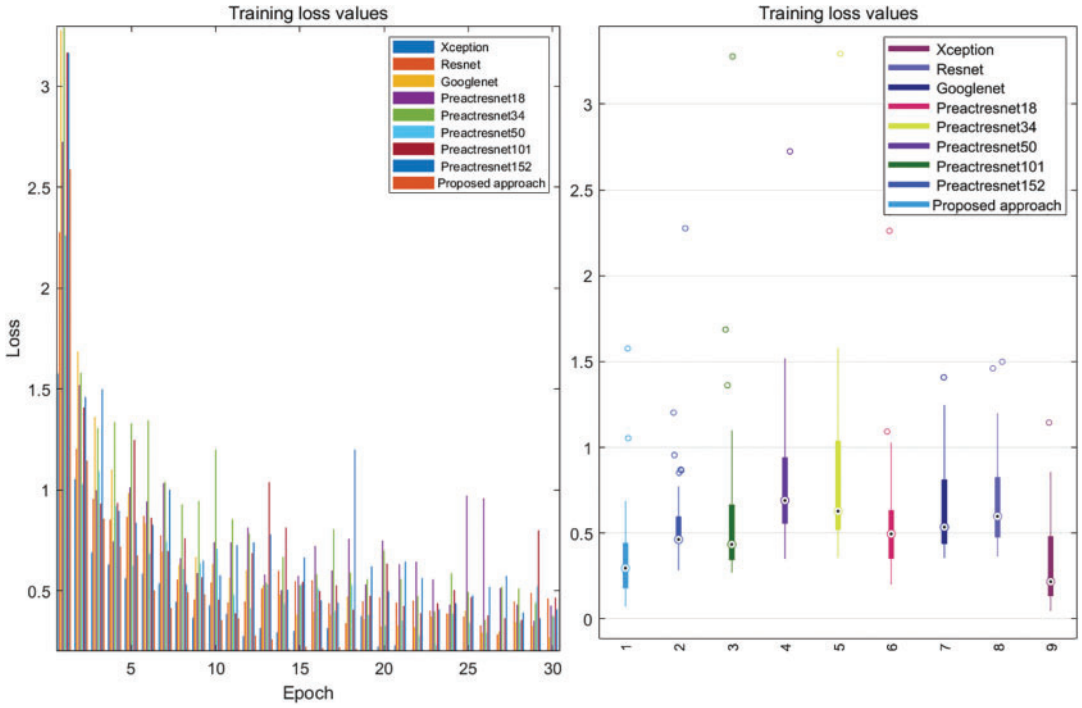

Figure 7: Loss of the deep learning models on training dataset

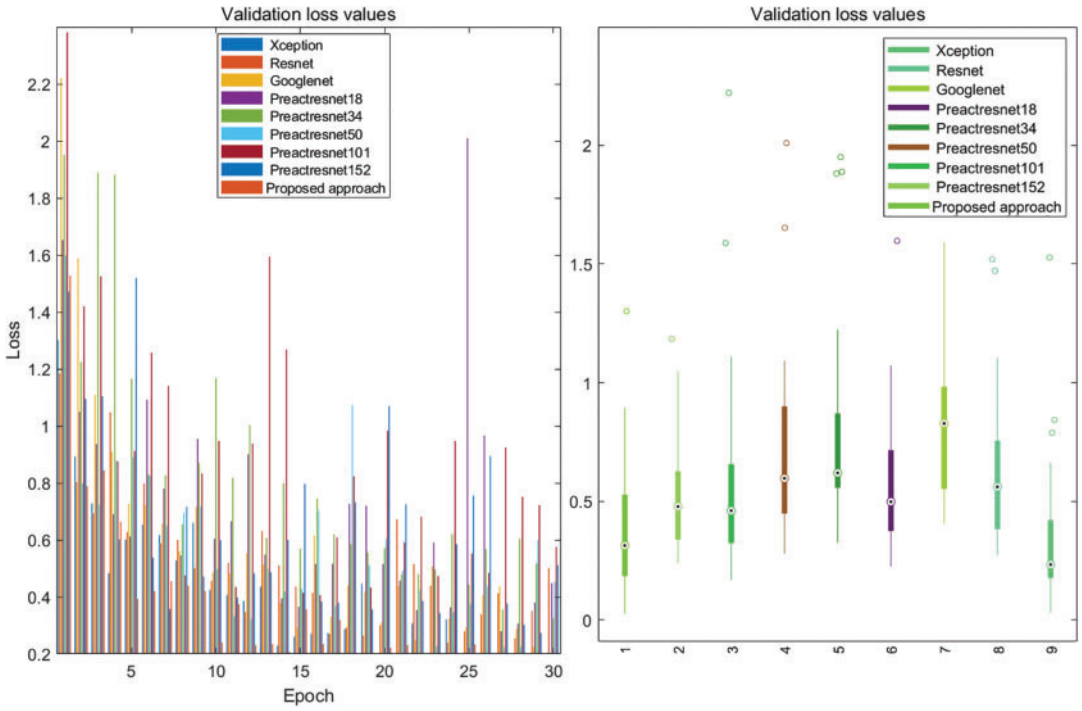

Figure 8: Loss of the deep learning models on validation dataset

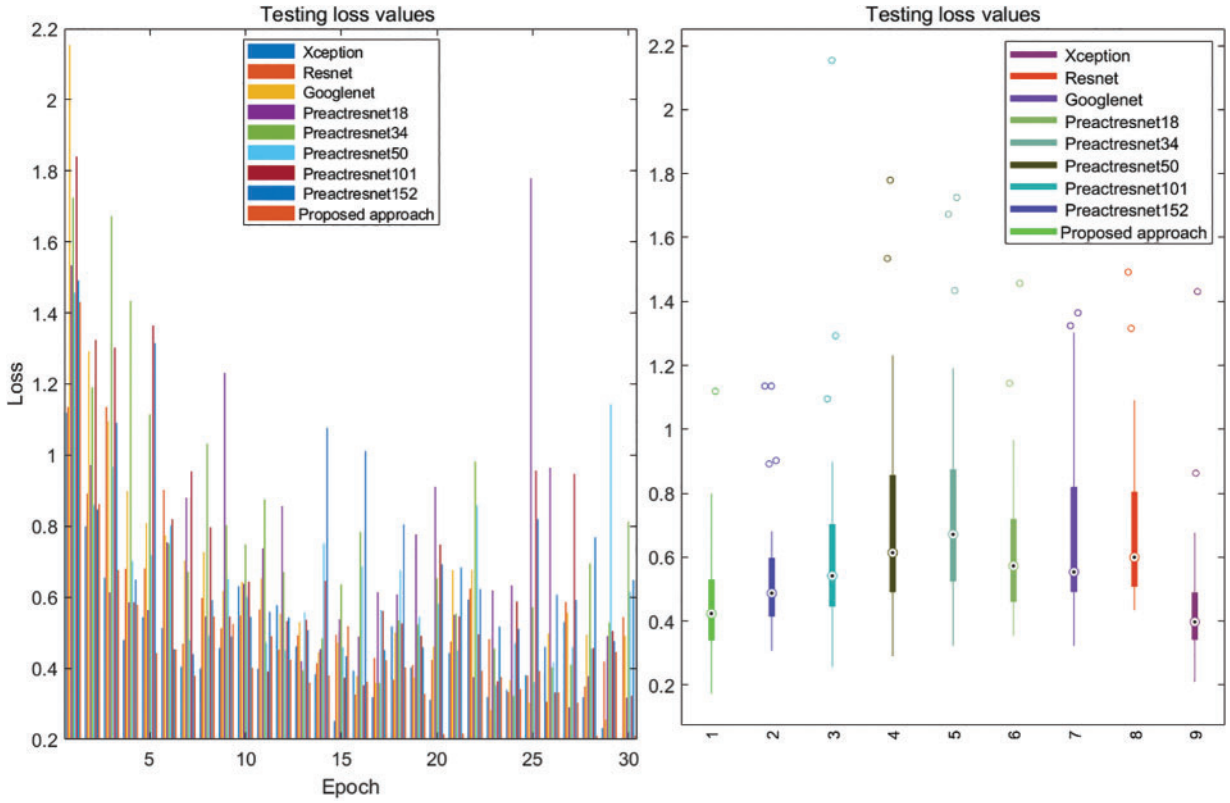

Figure 9: Loss of the deep learning models on testing dataset

The classification challenge posed by this dataset is more difficult than the classification challenge posed by ordinary industrial motor classification detection due to factors such as subtle interclass differences between different categories and intra-class differences with high feature duplication and redundancy (high feature repeatability). Fig. 10 shows the training, validation, and testing accuracy of the deep learning models over 30 evolution epochs. The loss and accuracy on the training, validation, and testing datasets are shown in Fig. 11. The learning rate in the model configuration is 0.001 with 30 epochs, and the cross-entropy loss between input logits and target is computed and used in the experiments, which is especially useful for unbalanced training sets. Adam combines the best properties of the AdaGrad and RMSProp algorithms in the model architecture optimization, which is chosen as the optimization based on stochastic gradient descent for training deep residual networks to handle sparse gradients on noisy problems.

The thermographic images of 11 IMs fault defects caused by coil faults (1, 2 and 3-phase, 10%, 30%, and 50%-stator rate of short-circuit) are extremely similar as shown in Figs. 2 and 3, and the differentiation of different textures, colors, and shapes is low, especially the attitude, implying that high-precision fault detection models are difficult to establish. Although image segmentation can be accomplished using an image cable connection with similar channel properties, the final segmentation area can be obtained. However, because of the low interclass similarity of IMs thermographic images, it is impossible to effectively improve feature distinguishability. As described in Eq. (7), we processed the image using Gaussian filtering and cascade the original image features, thereby combining the image's low-level features with rich position and detailed information and high-level features with

semantic information. Deep residual neural networks are coupled to create a high-precision fault identification model. Preprocessed graphics, as seen in Fig. 3, feature colors that are more intense and saturated, textures that are more distinct and detailed, and shapes that are more effective, all of which suggest more intricate expression in color, texture, and shape. The performance comparison of all the considered models is qualitatively given by Table 2. In comparison to Xception [24], Resnet [25], Karvelis et al. [26], Googlenet [27], Preactresnet18 [28], Preactresnet34 [28], Preactresnet50 [28], Preactresnet101 [28], Preactresnet152 [28], Najafi et al. [29], and Ahmed et al. [30], Preactresnet18 [28], Preactresnet34 [28], IMs' fault detection accuracy of the proposed approach is higher by 4%, 10%, 20.8%, 4%, 10%, 9%, 8%, 9%, 13%, 0.2%, and 2.33%, respectively. Based on the outlined discussion, the filtered low-level features are fused with the original features in a process known as "fusion" to enhance the image's color, texture, and form characteristics while precisely highlighting the location, detail, and high-level features. The performance of the proposed approach based on a deep residual network combined with feature fusion outperformed the excellent classification-detection approach to extract the image's high-discrimination features and construct the high-accuracy classification-detection approach for non-invasive fault diagnosis of IMs. Even the eleven deployed deep learning models' training, validation, and testing losses meet industry standards.

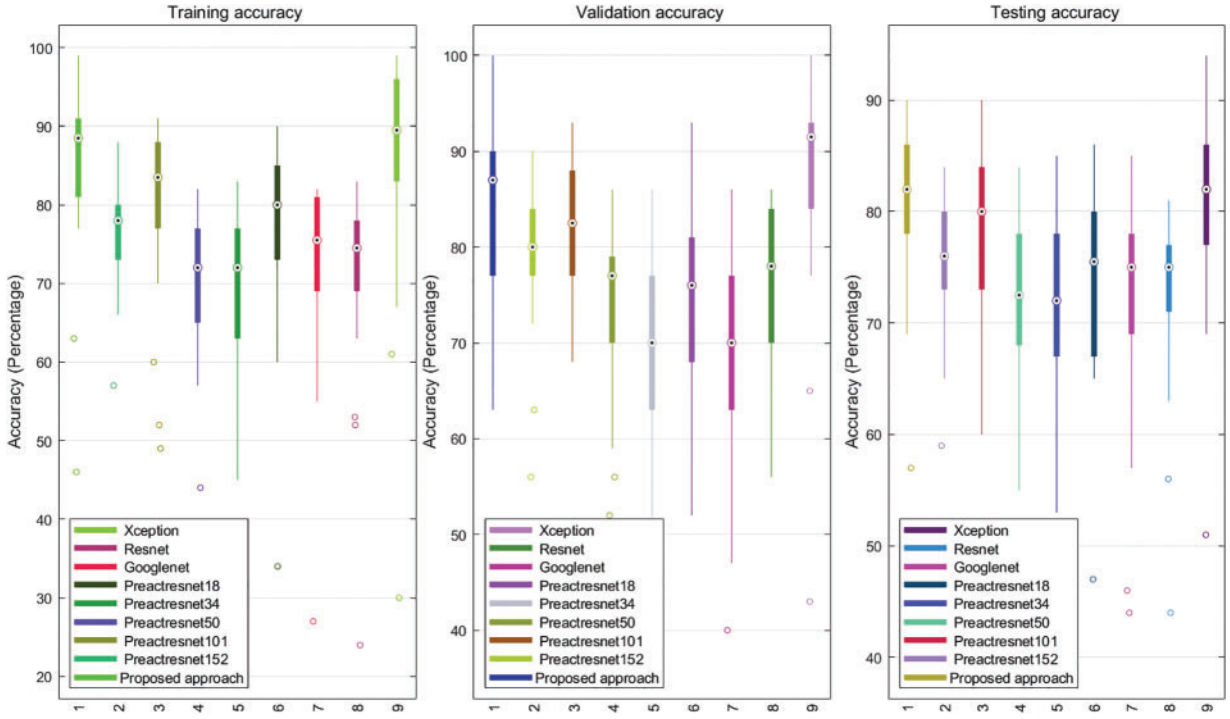

Figure 10: Training, validation, and testing accuracy of the nine deep learning models

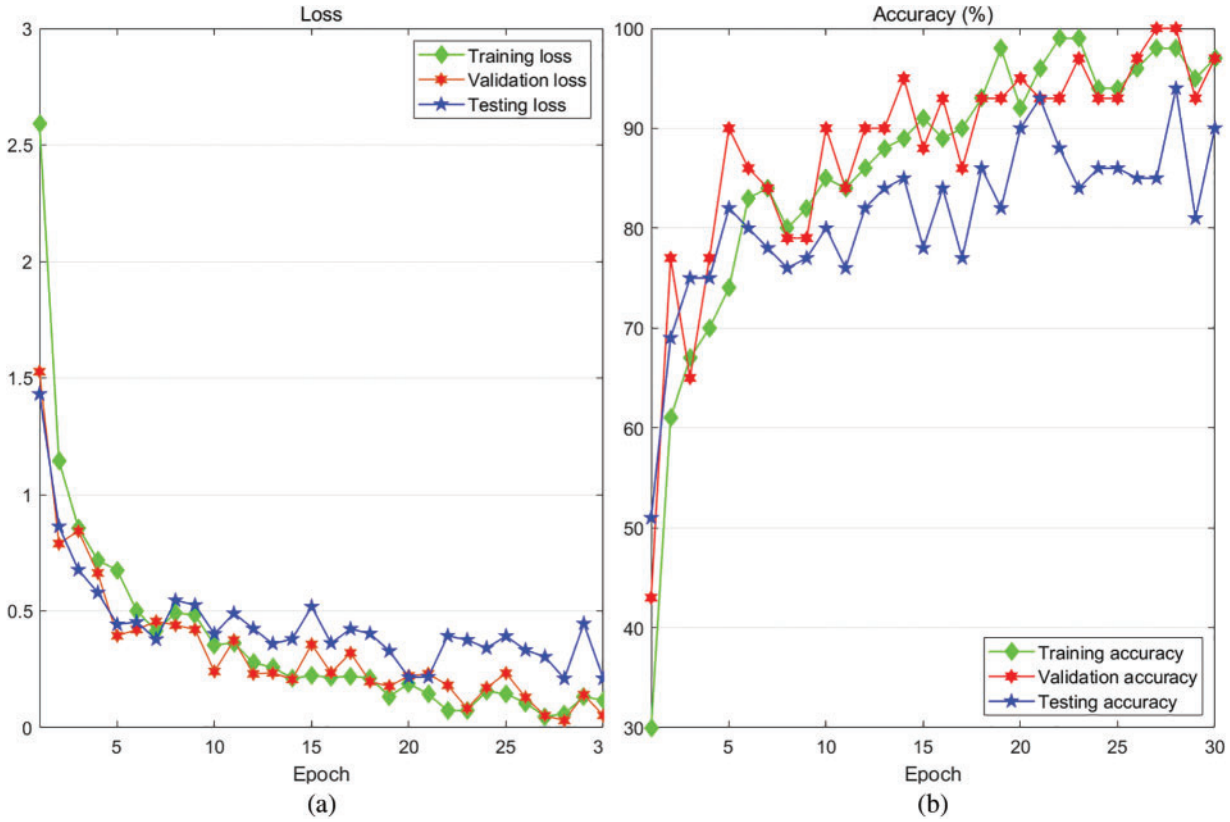

Figure 11: Performance of the proposed approach. (a) Loss of training, validation, and testing dataset; (b) Accuracy of training, validation, and testing dataset

Table 2: Performance comparison

Models	Train.loss	Val.loss	Test.loss	Train.acc	Val.acc	Test.acc
Xception [24]	0.3780	0.3941	0.4603	99%	100%	90%
Resnet [25]	0.6066	0.5095	0.5476	88%	90%	84%
Karvelis et al. [26]	N/A	N/A	N/A	N/A	N/A	73.2%
Googlenet [27]	0.6563	0.5787	0.6348	91%	93%	90%
Preactresnet18 [28]	0.7815	0.698	0.704	82%	86%	84%
Preactresnet34 [28]	0.8541	0.8076	0.7599	83%	86%	85%
Preactresnet50 [28]	0.5720	0.5780	0.6354	90%	93%	86%
Preactresnet101 [28]	0.7208	0.8792	0.6951	82%	86%	85%
Preactresnet152 [28]	0.7618	0.6437	0.6901	83%	86%	81%
Najafi et al. [29]	N/A	N/A	N/A	N/A	N/A	93.8%
Ahmed et al. [30]	N/A	N/A	N/A	N/A	N/A	91.67%
Proposed approach	0.3860	0.3348	0.4473	99%	100%	94%

5 Conclusion

This paper proposes a deep-learning-based approach for IM fault diagnosis that blends high-level features with more semantic information with low-level image features with higher resolution, more location, and more details. First, the publicly available dataset is preprocessed with the Gaussian filter, which is defined by thermal images produced by various short circuits and minor interclass distinctions between categories. Second, feature cascade is used to achieve the fusion of different scale features, which improves the distinguishability of features and characteristics in the dataset. Finally, the proposed approach achieved 99%, 100%, and 94% on the training, validation, and testing datasets, respectively, based on the publicly available IRT dataset used to demonstrate the condition monitoring of electrical equipment (IMs). Even when compared to existing methods and benchmark approaches, the method described in this paper can still achieve high prediction accuracy, and future work in this paper will continue to focus on high-precision fault diagnosis methods for industrial motors. Because the current dataset is provided through images, many variables related to operation conditions, such as full mechanical loads on the induction motor axis, different broken bar defects, the rotor circuit's current flow, stator current, rotor bar currents, ring current, rotor speed, rotor position, and target classes, cannot be effectively reflected and considered in deep learning models. Future research in this paper will focus on the variables and factors in electrical and mechanical signals, including the working conditions, in order to detect industrial motor faults more accurately and reasonably.

Acknowledgement: The authors would like to thank the editors and two anonymous reviewers for their constructive comments and insightful comments.

Funding Statement: This project is supported by the National Natural Science Foundation of China (No. 62001197), National High Technology Research and Development Program (863 Program) (2011AA05A107), Natural Sciences Research Grant for Colleges and Universities of Jiangsu Province (No. 22KJD470002) and Jiangsu Provincial Postgraduate Research and Practice Innovation Program (No. XSJCX21_58).

Conflicts of Interest: The authors declare that they have no conflicts of interest to report regarding the present study.

References

1. Huo, Z., Martínez-García, M., Zhang, Y., Yan, R., Shu, L. (2020). Entropy measures in machine fault diagnosis: Insights and applications. *IEEE Transactions on Instrumentation and Measurement, 69(6),* 2607–2620. https://doi.org/10.1109/TIM.2020.2981220
2. Elhaija, W. A., Al-Haija, Q. A. (2022). A novel dataset and lightweight detection system for broken bars induction motors using optimizable neural networks. *Intelligent Systems with Applications,* 200167. https://doi.org/10.1016/j.iswa.2022.200167
3. Zhang, S., Zhang, S., Wang, B., Habetler, T. G. (2020). Deep learning algorithms for bearing fault diagnostics–A comprehensive review. *IEEE Access, 8,* 29857–29881. https://doi.org/10.1109/ACCESS.2020.2972859
4. Glowacz, A. (2021). Fault diagnosis of electric impact drills using thermal imaging. *Measurement, 171(1–4),* 108815. https://doi.org/10.1016/j.measurement.2020.108815
5. Lu, S., Gao, Z., Xu, Q., Jiang, C., Zhang, A. et al. (2022). Class-imbalance privacy-preserving federated learning for decentralized fault diagnosis with biometric authentication. *IEEE Transactions on Industrial Informatics, 18(12),* 9101–9111. https://doi.org/10.1109/TII.2022.3190034

6. Xu, Q., Lu, S., Jia, W., Jiang, C. (2020). Imbalanced fault diagnosis of rotating machinery via multi-domain feature extraction and cost-sensitive learning. *Journal of Intelligent Manufacturing, 31(6),* 1467–1481. https://doi.org/10.1007/s10845-019-01522-8
7. Choudhary, A., Goyal, D., Letha, S. S. (2020). Infrared thermography-based fault diagnosis of induction motor bearings using machine learning. *IEEE Sensors Journal, 21(2),* 1727–1734. https://doi.org/10.1109/JSEN.2020.3015868
8. Glowacz, A., Tadeusiewicz, R., Legutko, S., Caesarendra, W., Irfan, M. et al. (2021). Fault diagnosis of angle grinders and electric impact drills using acoustic signals. *Applied Acoustics, 179(5),* 108070. https://doi.org/10.1016/j.apacoust.2021.108070
9. Chen, J., Hu, W., Cao, D., Zhang, M., Huang, Q. et al. (2020). Novel data-driven approach based on capsule network for intelligent multi-fault detection in electric motors. *IEEE Transactions on Energy Conversion, 36(3),* 2173–2184. https://doi.org/10.1109/TEC.2020.3046642
10. Li, Y. B., Du, X. Q., Wan, F. Y., Wang, X. Z., Yu, H. C. (2020). Rotating machinery fault diagnosis based on convolutional neural network and infrared thermal imaging. *Chinese Journal of Aeronautics, 33(2),* 427–438. https://doi.org/10.1016/j.cja.2019.08.014
11. Karabacak, Y. E., Özmen, N. G., Gümüşel, L. (2022). Intelligent worm gearbox fault diagnosis under various working conditions using vibration, sound and thermal features. *Applied Acoustics, 186(4),* 108463. https://doi.org/10.1016/j.apacoust.2021.108463
12. He, Z., Saho, H., Zhong, X., Yang, Y., Cheng, J. (2020). An intelligent fault diagnosis method for rotor-bearing system using small labeled infrared thermal images and enhanced CNN transferred from CAE. *Advanced Engineering Informatics, 46(2),* 101150. https://doi.org/10.1016/j.aei.2020.101150
13. Choudhary, A., Mian, T., Fatima, S. (2021). Convolutional neural network based bearing fault diagnosis of rotating machine using thermal images. *Measurement, 176(4),* 109196. https://doi.org/10.1016/j.measurement.2021.109196
14. Shao, H., Xia, M., Han, G., Zhang, Y., Wan, J. (2020). Intelligent fault diagnosis of rotor-bearing system under varying working conditions with modified transfer convolutional neural network and thermal images. *IEEE Transactions on Industrial Informatics, 17(5),* 3488–3496. https://doi.org/10.1109/TII.2020.3005965
15. Shao, H., Li, W., Xia, M., Zhang, Y., Shen, C. et al. (2021). Fault diagnosis of a rotor-bearing system under variable rotating speeds using two-stage parameter transfer and infrared thermal images. *IEEE Transactions on Instrumentation and Measurement, 70,* 1–11. https://doi.org/10.1109/TIM.2021.3111977
16. Gangsar, P., Tiwari, R. (2020). Signal based condition monitoring techniques for fault detection and diagnosis of induction motors: A state-of-the-art review. *Mechanical Systems and Signal Processing, 144(4),* 106908. https://doi.org/10.1016/j.ymssp.2020.106908
17. Nath, A. G., Udmale, S. S., Singh, S. K. (2021). Role of artificial intelligence in rotor fault diagnosis: A comprehensive review. *Artificial Intelligence Review, 54(4),* 2609–2668. https://doi.org/10.1007/s10462-020-09910-w
18. Gundewar, S. K., Kane, P. V. (2021). Condition monitoring and fault diagnosis of induction motor. *Journal of Vibration Engineering & Technologies, 9(4),* 643–674. https://doi.org/10.1007/s42417-020-00253-y
19. Jiao, J., Zhao, M., Lin, J., Liang, K. (2020). A comprehensive review on convolutional neural network in machine fault diagnosis. *Neurocomputing, 417(4),* 36–63. https://doi.org/10.1016/j.neucom.2020.07.088
20. Kaplan, K., Kaya, Y., Kuncan, M., Minaz, M. R., Ertunç, H. M. (2020). An improved feature extraction method using texture analysis with LBP for bearing fault diagnosis. *Applied Soft Computing, 87(6),* 106019. https://doi.org/10.1016/j.asoc.2019.106019
21. Yu, J., Zhang, C., Wang, S. (2021). Multichannel one-dimensional convolutional neural network-based feature learning for fault diagnosis of industrial processes. *Neural Computing and Applications, 33(8),* 3085–3104. https://doi.org/10.1007/s00521-020-05171-4

22. Akhil Vinayak, B., Anjali Anand, K., Jagadanand, G. (2020). Wavelet-based real-time stator fault detection of inverter-fed induction motor. *IET Electric Power Applications, 14(1),* 82–90. https://doi.org/10.1049/iet-epa.2019.0273
23. Najafi, M., Baleghi, Y., Mirimani, S. M. (2020). Thermal image of equipment (Induction Motor). *Mendeley Data,* V1. https//doi.org/10.17632/m4sbt8hbvk.1
24. Chollet, F. (2017). *Xception: Deep learning with depthwise separable convolutions*. Ithaca, NY, USA: Cornell University Press. https://arxiv.org/abs/1610.02357
25. Chollet, F. (2017). Xception: Deep learning with depthwise separable convolutions. *Proceedings of the IEEE Conference on Computer Vision and Pattern Recognition (CVPR)*, pp. 1251–1258. Honolulu, Hawaii.
26. Karvelis, P., Georgoulas, G., Stylios, C. D., Tsoumas, I. P., Antonino-Daviu, J. A. et al. (2014). An automated thermographic image segmentation method for induction motor fault diagnosis. *IEEE IECON 2014–40th Annual Conference of the IEEE Industrial Electronics Society*, pp. 3396–3402. Dallas, TX, USA.
27. Han, S., Pool, J., Tran, J., Dally, W. (2015). Learning both weights and connections for efficient neural network. *Advances in Neural Information Processing Systems, 28,* 1–9.
28. Sandler, M., Howard, A., Zhu, M., Zhmoginov, A., Chen, L. C. (2018). MobileNetV2: Inverted residuals and linear bottlenecks. *Proceedings of the IEEE Conference on Computer Vision and Pattern Recognition (CVPR)*, pp. 4510–4520. Salt Lake City, Utah.
29. Najafi, M., Baleghi, Y., Gholamian, S. A., Mirimani, S. M. (2020). Fault diagnosis of electrical equipment through thermal imaging and interpretable machine learning applied on a newly-introduced dataset. *IEEE 2020 6th Iranian Conference on Signal Processing and Intelligent Systems (ICSPIS)*, pp. 1–7. Mashhad, Iran.
30. Ahmed, M. M., Huda, A. N., Isa, N. A. M. (2015). Recursive construction of output-context fuzzy systems for the condition monitoring of electrical hotspots based on infrared thermography. *Engineering Applications of Artificial Intelligence, 39(2),* 120–131. https://doi.org/10.1016/j.engappai.2014.11.010